HHS Public Access

Author manuscript

Mol Cell. Author manuscript; available in PMC 2021 October 01.

Published in final edited form as:

Mol Cell. 2020 October 01; 80(1): 59–71.e4. doi:10.1016/j.molcel.2020.08.001.

Structural Basis of the Activation of Heterotrimeric Gs-protein by Isoproterenol-bound β_1-Adrenergic Receptor

Minfei Su[1,*], **Lan Zhu**[2,*], **Yixiao Zhang**[3,*], **Navid Paknejad**[4,*], **Raja Dey**[1], **Jianyun Huang**[1], **Ming-Yue Lee**[2], **Dewight Williams**[2], **Kelsey D. Jordan**[5], **Edward T. Eng**[5], **Oliver P. Ernst**[6,7], **Joel R. Meyerson**[1], **Richard K. Hite**[4], **Thomas Walz**[3], **Wei Liu**[2,§], **Xin-Yun Huang**[1,8,§]

[1]Department of Physiology and Biophysics, Weill Cornell Medical College of Cornell University, New York, NY 10065

[2]School of Molecular Sciences and Biodesign Center for Applied Structural Discovery, Arizona State University, Tempe, AZ 85287

[3]Laboratory of Molecular Electron Microscopy, The Rockefeller University, New York, NY 10065

[4]Structural Biology Program, Memorial Sloan Kettering Cancer Center, New York, NY 10065

[5]Department of Biochemistry, University of Toronto, Toronto, ON M5S 1A8, Canada

[6]Simons Electron Microscopy Center, New York Structural Biology Center, New York, NY 10027

[7]Department of Molecular Genetics, University of Toronto, Toronto, ON M5S 1A8, Canada

[8]Lead Contact

SUMMARY

Cardiac disease remains the leading causes of morbidity and mortality worldwide. The β_1-adrenergic receptor (β_1-AR) is a major regulator of cardiac functions and is down-regulated in the majority of heart failure cases. A key physiological process is the activation of heterotrimeric G-protein Gs by β_1-ARs, leading to increased heart rate and contractility. Here we use cryo-electron microscopy and functional studies to investigate the molecular mechanism by which β_1-AR activates Gs. We find that the tilting of α5-helix breaks an ionic lock between the sidechain of His373 in the C-terminal α5-helix and the backbone carbonyl of Arg38 in the N-terminal αN-

[§]To whom correspondence should be addressed. w.liu@asu.edu; xyhuang@med.cornell.edu.
[*]These authors contributed equally to this work.

AUTHOR CONTRIBUTIONS: M.S. expressed and purified β_1-AR, $G\alpha_s$, $G\beta_1\gamma_2$, Nb35 and the protein complexes, made cryo-EM grids, performed cryo-EM screening, data collection, image processing, and determined the EM density map. L.Z. made cryo-EM grids and performed data collection and image processing, as well as functional studies of the mutant β_1-ARs. Y.Z. made cryo-EM grids and performed image processing and determined the EM density map under the supervision of T.W. N.P. and R.K.H. performed image processing and determined the EM density map of the data presented in the final version of this paper. R.D. and J. R. M. performed image processing. J. H. generated the β_1-AR and Gs constructs. M.L. and D.W. performed data collection. K.D.J. and E.T.E. performed negative-stain EM and data collection. O.P.E. provided advice regarding experimental design and manuscript review and editing. W.L. supervised the project, and performed data collection and interpretation. X.Y.H. supervised the project, interpreted data and wrote the manuscript. All authors contributed towards the final version of the manuscript.

DECLARATION OF INTERESTS: The authors declare no competing interests.

helix of $G\alpha_s$. Together with the disruption of another interacting network involving Gln59 in the α1-helix, Ala352 in the β6-α5 loop, and Thr355 in the α5-helix, these conformational changes might lead to the deformation of the GDP-binding pocket. Our data provide molecular insights into the activation of G-proteins by G-protein-coupled receptors.

Graphical Abstract

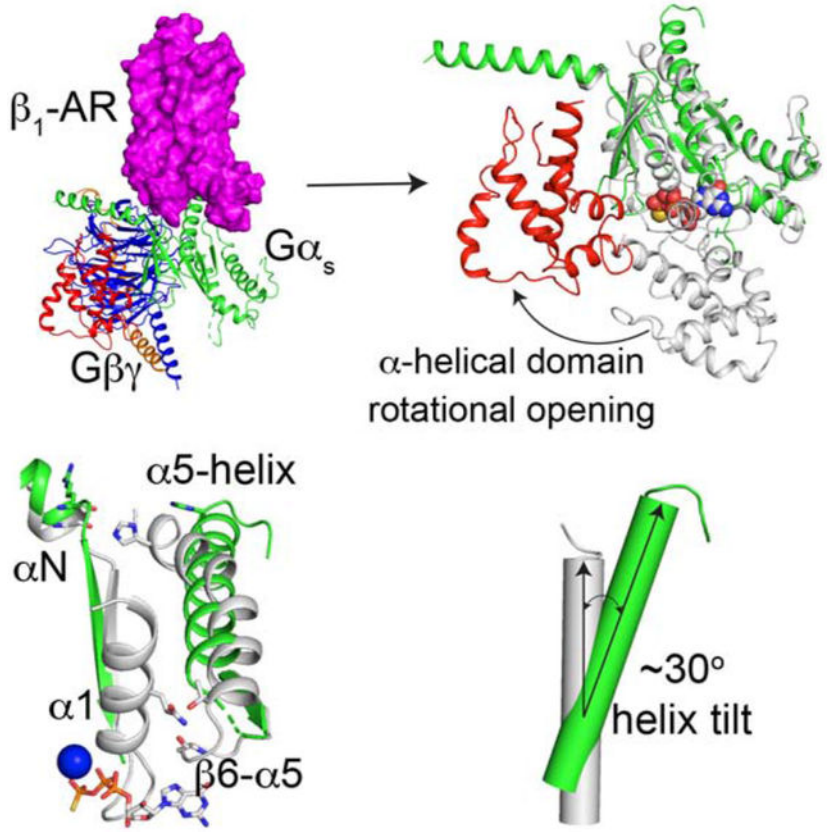

eTOC Blurb:

Su et al. report the cryo-EM structure of the complex of isoproterenol-bound β_1-adrenergic receptor and heterotrimeric Gs-protein. The structural and functional studies reveal insights into the activation of Gs by β_1-adrenergic receptor. This work advances our understanding of the control of heart rate and contractility by the nervous system and hormones.

INTRODUCTION

A structurally diverse repertoire of ligands elicit their physiological functions by activating G-protein-coupled receptors (GPCRs) (Fredriksson et al., 2003; Rosenbaum et al., 2009; Sakmar, 2002; Strange, 2008; Weis and Kobilka, 2018). GPCRs comprise a large and diverse superfamily of transmembrane proteins, and family members have been identified in organisms as evolutionarily distant as yeast and human. Critically, GPCRs constitute the protein class that has been most successfully targeted by drugs, and accordingly are the focus of intense mechanistic study (Strange, 2008). Canonically, GPCRs signal directly to

heterotrimeric G-proteins which in turn relay the signals to downstream pathways (Bourne et al., 1990; Gilman, 1987; Simon et al., 1991). These G-proteins are composed of Gα, Gβ, and Gγ subunits, with the Gβ and Gγ subunits tightly associating such that they can be regarded as one functional unit (Gβγ). G-proteins function as molecular binary switches with their biological activity determined by the bound nucleotide (Lappano and Maggiolini, 2012; Oldham and Hamm, 2008; Sprang, 1997). Activated GPCRs function as a guanine-nucleotide exchange factor (GEF), promoting the release of GDP bound on the Gα subunit of G-proteins and creating the thermally labile, transition state of Gα without a bound nucleotide (Bourne, 1997). The subsequent binding of GTP leads to the dissociation of the Gα subunit from the Gβγ dimer resulting in two functional subunits (Gα and Gβγ). Both the Gα and Gβγ subunits signal to various cellular pathways. Based on the sequence and functional homologies, G-protein heterotrimers are categorized into four families: G_s, G_i, G_q, and $G_{12/13}$ (Simon et al., 1991). The molecular mechanisms by which GPCRs activate these G-proteins are incompletely understood.

The β_1-adrenergic receptor (β_1-AR) is a member of the GPCR family. In the adult human heart, β_1-AR is the predominantly expressed β-AR isoform (70~85%) (Benovic, 2002; Post et al., 1999). The receptor binds and is activated by the catecholamines, norepinephrine and epinephrine, which triggers Gs-protein activation and increased cardiac cAMP levels. These molecular events manifest physiologically as increased heart rate, increased conduction, reduced refractoriness within the atrioventricular node, increased contractility and increased cardiac output (Lohse et al., 2003). Down-regulation of β_1-ARs has been described in most cases of heart failure which is one of the main causes of mortality in the developed world (Lohse et al., 2003). Inhibitors of β-ARs (beta-blockers) are used to treat high blood pressure and heart failure, to manage abnormal heart rhythms, and to protect against myocardial infarction (Frishman, 2008). The molecular mechanism by which β_1-AR catalyzes the guanine-nucleotide exchange on Gs, thus activating Gs, is not completely clear. Here we use cryo-electron microscopy and functional studies to investigate the activation of Gs by β_1-AR. We find that, during its activation by isoproterenol-bound β_1-AR, the α-helical domain of Gs rotates away from its Ras-like domain. The rotational opening of the α-helical domain is by ~96° and the distance between mass centers is ~38 Å. These rotation angle and translational distance are different from those observed in the crystal structure of the BI-167107 (a high affinity agonist)-bound β_2-AR–Gs complex. This α-helical domain rotation, together with the structural rearrangements (including the tilting) in the C-terminal α5-helix and the GDP-binding pocket, result in the GDP release. These results provide structural insights into the activation of Gs by β_1-AR.

RESULTS AND DISCUSSION

Molecular recognition of Gs by β_1-AR

To understand the molecular mechanism by which β_1-AR activates Gs, we first investigated how β_1-AR recognizes Gs during the activation process. We solved the cryo-EM structure of the complex of isoproterenol-bound β_1-AR and Gs, at an overall resolution of 2.6 Å (Figure 1, Figures S1 and S2, Table 1). As revealed by this structure, β_1-AR recognizes both $G\alpha_s$ (1049 $Å^2$ buried area) and Gβ (153 $Å^2$ buried area), yielding a large interaction surface area

(1202 Å^2) (Figures 1 and 2, Figure S3). On β_1-AR, the interacting elements involve transmembrane domain (TM) 3, TM5, TM6, and intracellular loop (ICL) 2 (Figure 2 A-D, Figure S4). On Gα_s, the N-terminal αN-helix and its structurally adjacent regions (the αN-β1 loop and the β2-β3 loop), as well as the C-terminal α5-helix are interacting with β_1-AR (Figure 2 A-D, Figure S4).

We first explored how β_1-AR undergoes structural changes to accommodate Gs binding, and then the structural changes on Gs upon β_1-AR interaction and during its activation process. Since the Gs interacting surface is on the cytoplasmic side of β_1-AR we focused on the structural changes of β_1-AR on its cytoplasmic side upon Gs binding (Figure 2 E-H). In the β_1-AR–Gs complex with the full agonist isoproterenol, β_1-AR adopts an active state conformation (Figure 2E). For comparative analysis between active and inactive state models, we used our new cryo-EM active state structure, and our previously reported β_1-AR inactive state structure (PDB: 4GPO) (Huang et al., 2013) (Figure 2 E-H). We note that this inactive state structure is globally similar to other reported structures resolved in the same functional state (Warne et al., 2008). Comparison of the models reveals salient conformational differences (Figure 2 E-H). The overall root-mean-square deviation between the structures of β_1-AR in the active and inactive states is ~3 Å over 276 Cα atoms. The largest structural changes upon Gs engagement occur in the cytoplasmic side of β_1-AR, with an outward rotation of TM6 by ~14 Å (measured at the Cα of Glu285), a helix extension in TM5, and an inward ~5 Å movement of TM7 (measured at the Cα of Tyr343) (Figure 2F).

Gs-bound active β_1-AR undergoes critical conformational changes in the conserved D(E)RY motif on TM3 and the conserved NPxxY motif on TM7 to recognize Gs (Figure 2 G and H). In the inactive β_1-AR structure, Arg139 within the D(E)RY motif forms a salt bridge (or the ionic lock) with Glu285 (on TM6) (Figure 2G). This salt bridge stabilizes the inactive state of family A GPCRs, although it is absent in the structure of the inactive state of β_2-AR (likely due to the high basal activity of β_2-AR) (Cherezov et al., 2007). In the active state of β_1-AR, this ionic lock is broken, and the C-terminal end of α5-helix of Gα_s occupies the space originally occupied by Glu285 in the inactive state (Figure 2G). The new position for Glu285 in the active state is ~14 Å outwards (Figure 2G). Arg139 (in TM3) now forms a packing interaction with Tyr377 in the α5-helix of Gα_s (Figure 2G). Furthermore, TM7 rotates around the conserved motif NPxxY (Figure 2H). This moves Tyr343 toward the position that was occupied by TM6 in the inactive structure (Figure 2H). Also, the last turn of the helix in TM7 in the inactive structure unravels in the active β_1-AR, and TM7 has a small inward movement (Figure 2H). Therefore, β_1-AR recognizes Gs by forming extensive interactions with Gs. Reciprocally, Gs binding stabilizes the structural changes in the active β_1-AR by moving into places originally occupied by the inactive β_1-AR.

Structural rearrangements of the C-terminal α5-helix of Gα_s.

After examining how β_1-AR undergoes structural changes to recognize Gs during Gs activation by β_1-AR, we next explored the structural changes on Gs after its interaction with β_1-AR. Both the N-terminal αN-helix and the C-terminal α5-helix of Gα_s are critically involved in interacting with β_1-AR (Figures 1 and 2). We examined the C-terminal α5-helix first since it contributes most of the interacting buried surface, suggesting that interactions in

this region provide the major binding energy for the formation of the complex (Figure 3A). β_1-AR primarily uses the surface formed by TM3, TM5, TM6, and ICL2 to interact with Gs (Figure 3A). This surface resembles a saddle that cradles the C-terminal α5-helix of the Ras-like domain of $G\alpha_s$ (Figure 3A). The C-terminal tail of the α5-helix is critical for GPCR–G-protein coupling specificity, and replacement of the last four amino acid residues of $G\alpha_q$ by $G\alpha_i$ enabled Gq to couple to an otherwise Gi-coupled GPCR (Conklin and Bourne, 1993; Conklin et al., 1993). The last four amino acids (Tyr377 to Leu380) of $G\alpha_s$ form a C-terminal α_L capping motif which stabilizes helix ends, prevents helix fraying and imposing a substantial restriction on the set of allowed conformations (Aurora and Rose, 1998; Aurora et al., 1994)(Figure 3B). This capping motif interacts extensively with the cytoplasmic ends of TM3 and TM6 (Figure 3 C-E).

The comparison of the α5-helix in the complex of β_1-AR–Gs and in the $G\alpha_s$ alone ($G\alpha_s$:GTPγS) structure determined by X-ray crystallography (PDB: 1AZT) reveals significant structural rearrangements of the α5-helix during Gs activation by β_1-AR (Figure 3 F and G). In $G\alpha_s$ alone, the last 3 amino acid residues (E378 to L380) of the C-terminal capping motif of α5-helix were disordered and unresolved in the structure (Figure 3F). In the β_1-AR–Gs complex, residues L374 to Q376 form a helix extension and interact extensively with β_1-AR (Figure 3 C-E). These additional helix extension and translation extend α5-helix by ~6 Å. Furthermore, α5-helix undergoes a rotation around Phe362 (Figure 3F). In addition, there is a tilting by ~30° of the α5-helix from its position in $G\alpha_s$ alone to the position in the β_1-AR–Gs complex (Figure 3 F and G). The helix tilting, together with the helix extension and rotation, might provide α5-helix as a molecular force buffer transducing β_1-AR signal to the GDP/GTP-binding pocket. Computational simulations indicate that α5-helix conformation changes are mainly associated with GDP release (Dror et al., 2015). Hence the structural rearrangements of the C-terminal α5-helix of $G\alpha_s$ upon β_1-AR binding are critical to the guanine-nucleotide exchange on Gs.

Rotational opening of α-helical domain of Gs

Gα subunits consist of two domains: a Ras-like GTPase domain and an α-helical domain (Dohlman and Jones, 2012; Sprang et al., 2007) (Figure 4 A and B). These two domains are connected by Linkers 1 and 2. Between these two domains lies a deep cleft within which GDP or GTP is tightly bound. The nucleotide is essentially occluded from the bulk solvent (Coleman et al., 1994; Noel et al., 1993). Comparing the conformation of $G\alpha_s$ in our β_1-AR–Gs complex structure with the crystal structure of $G\alpha_s$ alone (PDB: 1AZT) (Sunahara et al., 1997) (Figure 4B), the principal change is a large rotation of the α-helical domain by ~96° (Figure 4, A and B). The distance between mass centers is ~38 Å (Figure 4B). The maximum rotation was limited by the presence of Gβγ, and the rotated α-helical domain was in contact with Gβγ and could not rotate any further (Figure 4 C and D). Hence, the observed location of the α-helical domain in the β_1-AR–Gs complex likely represents the fully open state (Figure 4, C and D). From all the reported structures of the complexes of GPCR–G-protein trimers, only two structures include the α-helical domains of Gα subunits (Draper-Joyce et al., 2018; Kang et al., 2018; Koehl et al., 2018; Liang et al., 2018; Liang et al., 2017; Rasmussen et al., 2011; Zhang et al., 2017). The positions of the α-helical domains in these two structures are different from that observed in the β_1-AR–Gs structure

reported here (Figure 5). A comparison between the isoproterenol-bound β_1-AR–Gs and the crystal structure of BI-167107-bound β_2-AR–Gs (PDB: 3SN6) reveals that, in β_2-AR–Gs, the α-helical domain appears to rotate farther towards the receptor and the membrane (Figure 5 A and B). This difference might be due to the crystal lattice contact in the crystal structure of β_2-AR–Gs (Hilger et al., 2018). In the constitutively active rhodopsin–Gi structure, the α-helical domain is also in a different position from the α-helical domain in β_1-AR–Gs; this might be due to the different G-proteins used (Gs vs. Gi) or the utilization of an antibody to bind and stabilize the α-helical domain and Gβ simultaneously in the rhodopsin–Gi structure (Kang et al., 2018) (Figure 5 A and B). It is worth noting that the relatively weak density for the α-helical domain in the EM map suggests the dynamic nature of the α-helical domain. Hence, the structural data point to the rotational opening of the α-helical domain during G-protein activation that creates an egress route for GDP.

Deformation of the GDP-binding pocket

In the β_1-AR–Gs complex, the GDP/GTP binding pocket is conformationally deformed, and the pocket is empty without GDP. Relative to the Ras-like domain in the structure of $G\alpha_s$:GTPγS, most of the conformational changes of the Ras-like domain in the complex of β_1-AR–Gs occur surrounding the GDP/GTP-binding pocket, while leaving the remainder of the Ras-like domain largely unperturbed (Figure 6 A-E). The modified regions include the P-loop (the β1-α1 loop, involved in binding of the diphosphate of the guanine nucleotide) (Figure 6 A), the TCAT motif (the β6-α5 loop, involved in the coordination of the purine ring of the bound nucleotide) (Figure 6D), and the Switch II and III regions (Figure 6 B and C). The cryo-EM map density for these modified regions is poor, indicating dynamic conformations. The binding between the β-phosphate of GDP and the P-loop is critical since GMP binds much weaker (~10^6-fold lower affinity) than GDP (John et al., 1990). In fact, GEFs for Ras-superfamily of GTPases promote GDP release by disrupting the interaction between the β-phosphate of GDP and the P-loop (Bos et al., 2007). In $G\alpha_s$:GTPγS, residues from the P-loop (including Glu50, Ser51, Gly52, Lys53, and Ser54) interact with the β-phosphate (Figure 6E). In the complex of β_1-AR–Gs, this region is disordered (Figure 6A). The disruption of this P-loop would markedly reduce the GDP binding. Hence β_1-AR likely promotes GDP release by disrupting the interaction between the β-phosphate of GDP and the P-loop. Furthermore, Thr190 in Linker 2 is involved in binding of the γ-phosphate of GTP (Figure 6E). In the β_1-AR–Gs structure, Linker 2 is disordered (Figure 4A). Additionally, Leu184 and Arg185 in αF-helix (part of the α-helical domain) interact with the pentose sugar in $G\alpha_s$:GTPγS, but move away as part of the α-helical domain during the rotational opening in the β_1-AR–Gs complex (Figure 6E, Figure 4A). Linker 2 and αF-helix are essential for GDP/GTP binding, and are also required to stabilize the GTP binding after GDP/GTP exchange, and to coordinate the γ-phosphate binding (Lambright et al., 1996; Wall et al., 1995). Therefore, the conformation of the GDP-binding pocket in β_1-AR–Gs complex is modified with the effect of weakening the interaction between GDP and $G\alpha_s$. This provides a structural basis for the release of GDP.

Moreover, the interacting network between the N-terminal part of $G\alpha_s$ and the C-terminal part of $G\alpha_s$ observed in the structure of $G\alpha_s$:GTPγS is broken in the structure of the β_1-AR–Gs complex (Figure 6F). In the $G\alpha_s$:GTPγS, there is an ionic lock between the

sidechain of His373 in the α5-helix and the backbone carbonyl of Arg38 in the αN-helix (Figure 6F). This contact would tighten together the N- and C-terminal ends of $G\alpha_s$. In the complex of β_1-AR–Gs, the tilting and translation of the α5-helix move His373 away and break this ionic lock (Figure 6F). Moreover, there is another interacting network involving Gln59 in the α1-helix in the structure of $G\alpha_s$ alone (Figure 6F). The sidechain of Gln59 forms a hydrogen bond with the backbone carbonyl of Ala352 in the β6-α5 loop, as well as interacts with the sidechain of Thr355 in the α5-helix (Figure 6F). In the complex of β_1-AR–Gs, this contacting network is broken, leading to the disordering of the α1-helix, the P-loop and the TCAT motif (Figure 6F). As these regions contribute to the majority of the binding of GDP (Figure 6 A, D and E) , the disruption of these regions would certainly lead to GDP release.

Functional studies of the activation of Gs by β_1-AR

From the structure of β_1-AR–Gs complex, there are two principle routes from β_1-AR to the GDP/GTP-binding pocket (Figures 1 and 2). One route is through the C-terminal α5-helix of $G\alpha_s$ and the β6–α5 loop which engages the guanine ring (Figure 6D). The role of α5-helix in G-protein activation by GPCRs has been well documented (Hilger et al., 2018). The second route is through ICL2 of β_1-AR which interacts with the N-terminal αN-helix (Figure 7A). This signal is transmitted through β1 to the P-loop which coordinates the β-phosphate of the guanine nucleotide (Figure 6A). From the β_1-AR–Gs structure, Arg38 in the N-terminal αN-helix of $G\alpha_s$ interacts with Gln150 in ICL2 of β_1-AR (Figure 7A). This interaction stabilizes a helical conformation of ICL2, which positions Pro146 and Phe147 in ICL2 to form hydrophobic interactions with Ile369, Arg366, and Phe362 in α5-helix, Val203 in the β_2-β_3 loop, and His41 in the αN-β1 loop of $G\alpha_s$ (Figure S4). For $G\alpha_{i1}$, the αN-β1 loop was shown to be critical for the nucleotide-exchange catalysis (Herrmann et al., 2006). We have performed functional studies of residues on β_1-AR that interact with $G\alpha_s$ based on our cryo-EM structure of the complex of β_1-AR and Gs. As shown in Figure 7 A and B, residues Pro146, Phe147, and Gln150 in ICL2 of β_1-AR are involved in interacting with $G\alpha_s$. Val230, Glu233, and Gln237 in TM5, as well as Thr291 in TM6 interact with the α5-helix of $G\alpha_s$. We mutated these residues to Ala, and the functions of these β_1-AR mutants were examined by their ability to activate Gs in cells as quantified by the cellular cAMP production (Figure 7, C-E). Comparing with wild-type β_1-AR, these β_1-AR mutants had reduced efficacy in activating Gs (Figure 7 C and D). These functional studies support our structural data, and confirm the importance of the β_1-AR–Gs interactions (revealed by the structural study) in the activation of Gs by β_1-AR.

CONCLUSION

We have investigated the structural basis for the activation of Gs by β_1-AR. The cryo-EM structure of the complex of β_1-AR–Gs reveals the conformation of the active state of β_1-AR, the molecular recognition of Gs by the active β_1-AR, the direct interaction between ICL2 of β_1-AR and the N-terminal αN-helix of $G\alpha_s$, and the structural changes of Gs upon the coupling to β_1-AR. The principal mechanism for β_1-AR as a GEF for Gs is to deform the GDP/GTP-binding pocket and to accelerate GDP release from Gs. β_1-AR induces a tilting of the α5-helix, the break of the ionic lock between His373 in the α5-helix and Arg38 in the

αN-helix, the disruption of the interacting networks involving Gln59 in the α1-helix, Ala352 in the β6-α5 loop, and Thr355 in the α5-helix, the rotational opening of the α-helical domain from the Ras-like domain, and the deformation of the GDP/GTP-binding pocket. All these conformational changes lead to the GDP release. It is worth noting that the Ras-like domain of $G\alpha_s$, purified as an isolated recombinant protein, had been shown to be able to bind to GDP and GTP, and to stimulate the activity of adenylyl cyclase which could be further enhanced by the addition of the separately purified recombinant α-helical domain of $G\alpha_s$ (Markby et al., 1993). Indeed, in the β_1-AR–Gs structure, even when the Ras-like and α-helical domains are separated, some of the residues involved in GDP/GTP binding do not change their relative locations (Figure 6E), thus providing the possibility of a subsequent binding of GTP (albeit weakly). This initial weak binding of GTP is likely strengthened by the subsequent re-closing of the α-helical domain. Reciprocally, GTP binding promotes the association of the Ras-like domain and the α-helical domain, and the α-helical domain accelerates GTP hydrolysis, thus completing one cycle of the guanine nucleotide-exchange on $G\alpha_s$. Altogether, our studies advance the understanding of Gs activation by β_1-AR, and the activation of G-proteins by GPCRs in general.

Limitations:

As shown in the local resolution map (Figure S2), the complex of isoproterenol–β_1-AR–Gs was well-resolved in most regions. However, similar to many other cryo-EM density maps, some regions of the map, including the α-helical domain of $G\alpha_s$, are weaker than other regions. This weak density reflects the highly dynamic nature of the α-helical domain in the nucleotide-free state. To interpret this density, the isoproterenol–β_1-AR–Gs density map was low-pass filtered to 6 Å and then the α-helical domain from the X-ray crystal structure of β_2-AR–Gs (PDB 3SN6) was manually docked and rigid-body refined. While the density for the α-helical domain is weaker and the high-resolution features are blurred out due to its increased disorder, it is not absent and its position is clearly resolved in the low-pass filtered map. Without high-resolution features, we are limited in modeling its structure to rigid-body fitting into the low-pass filtered map. Therefore, we only used the information about the relative position of the α-helical domain of $G\alpha_s$ in the complex in this paper and future studies will be required to understand the dynamics of the α-helical domain of Gα.

STAR★Methods

RESOURCE AVAILABILITY

LEAD CONTACT—Further information and requests for resources and reagents should be directed to and will be fulfilled by the Lead Contact, Xin-Yun Huang (xyhuang@med.cornell.edu).

MATERIALS AVAILABILITY—All unique reagents generated in this study will be made available on request by the Lead Contact with a completed Materials Transfer Agreement (MTA).

DATA AND CODE AVAILABILITY—The cryo-EM reconstructions of the isoproterenol–β_1-AR–Gs complex have been deposited in the Electron Microscopy Data Bank (EMDB)

under ID codes EMDB: EMD-22357. The corresponding atomic model has been deposited in the Protein Data Bank (PDB) under ID codes PDB: 7JJO.

EXPERIMENTAL MODEL AND SUBJECT DETAILS—Turkey β_1-AR, bovine Gβ_1 and bovine Gγ_2(C68S) were expressed in Sf9 insect cells (Expression Systems) infected with recombinant baculovirus. Bovine Gα_s and Nb35 were expressed in *E. coli* strain BL21(DE3) (New England Biolabs). CHO-K1 cells overexpressing wild-type and mutant β_1-ARs were used in cAMP functional assays.

METHODS DETAILS

Expression and purification of β_1-AR, Gα_s, Gβ_1, Gγ_2 and Nb35: β_1-AR protein was purified as described previously (Huang et al., 2013). The turkey β_1-AR construct β_1-AR(H12) used in this study was similar to the functional β_1-AR(H0) construct described previously with some modifications (Huang et al., 2013). A signal peptide, FLAG tag, PreScission protease cleavage site and T4 lysozyme were fused to the N-terminus with a doublealanine linker, and another PreScission protease cleavage site and His_6 tag were added to the C-terminus. β_1-AR was expressed and purified from Sf9 insect cells grown in ESF 921 protein-free medium (Expression Systems). Cells were grown to 2 to 3 million cells per ml before 200 ml of baculoviruses were added for infection. 48 hrs later, cells were harvested by centrifugation, flash frozen in liquid nitrogen and stored at −80 °C until use. For membrane preparation, cell pellets were lysed by sonication in a buffer containing 20 mM Tris, pH 8, 1 mM EDTA and protease inhibitor cocktail (Roche) and washed once more using the same buffer. Purified membranes were resuspended in 20 mM Tris, pH 8, 0.2 mM EDTA, and protease inhibitor cocktail and flash frozen in liquid nitrogen and stored at −80 °C. For protein purification, membrane preparations were first thawed in 20 mM Tris, pH 8, 350 mM NaCl, and protease inhibitor cocktail. 1 mM isoproterenol (Sigma) was then added and the mixture was stirred for 1 hr at 4 °C and the membranes were then solubilized in 20 mM Tris, pH 8, 350 mM NaCl, 1% n-Dodecyl-β-D-Maltopyranoside (DDM, Anatrace), 1 mM isoproterenol and protease inhibitor cocktail for 1 hr at 4°C. The DDM concentration was then reduced to 0.5% by adding equal volume of 20 mM Tris, pH 8, 350 mM NaCl, and 1 mM isoproterenol and the mixture was stirred for another 1 hr at 4°C. The preparation was clarified by ultracentrifugation at 142,000 g for 30 min at 8°C. The supernatant was then incubated with Ni-NTA resin (Qiagen) with stirring at 4 °C with 8 mM imidazole. After 4 hrs, the resin was collected by centrifugation and washed three times with 20 mM Tris, pH 8, 500 mM NaCl, 0.02% DDM, 1 mM isoproterenol, and 8 mM imidazole and one time with 20 mM Tris, pH 8, 100 mM NaCl, 0.02% DDM, 1 mM isoproterenol, and 8 mM imidazole. β_1-AR was then eluted from the resin with 20 mM Tris, pH 8, 100 mM NaCl, 0.02% DDM, 1 mM isoproterenol, and 120 mM imidazole. The elution was concentrated and further purified by size-exclusion chromatography using a Superdex 200 Increase 10/300 column (GE Healthcare) pre-equilibrated with 20 mM Tris, pH 8, 100 mM NaCl, 0.02% Lauryl Maltose Neopentyl Glycol (LMNG, Anatrace), 1 mM isoproterenol. Purified β_1-AR was concentrated to 4 mg/ml and either used immediately for complex assembly or flash frozen in liquid nitrogen and stored at −80 °C.

The recombinant wild-type bovine $G\alpha_s$ was purified from *E. coli* strain BL21(DE3) (New England Biolabs) (Huang et al., 2015). This $G\alpha_s$ construct had an N-terminal GST tag that was removable through a PreScission protease cleavage site. Cells were grown in 2×YT medium (MP Biomedicals) at 37 °C until OD_{600} reached 0.6. Protein expression was then induced by 75 μM IPTG (GoldBio) and continued for 16 hrs at 16 °C. Cells were harvested by centrifugation, flash frozen in liquid nitrogen and stored at −80 °C. For protein purification, cell pellets were thawed in a lysis buffer containing 20 mM HEPES, pH 7, 150 mM NaCl, 10% glycerol, 5 mM β-mercaptoethanol, 2 mM $MgCl_2$, 1 mM EDTA, 10 μM GDP (Sigma), 0.1 mg/ml lysozyme, 0.2 mM PMSF and protease inhibitor cocktail, and further lysed by sonication. Cell debris was removed by centrifugation at 20,000 g for 40 min 4 °C. Supernatant was then collected and incubated with Glutathione resin (Pierce) with stirring for 1 hr at 4 °C. Resin was then washed four times with 20 mM HEPES, pH 7, 150 mM NaCl, 10% glycerol, 5 mM β-mercaptoethanol, 2 mM $MgCl_2$, 1 mM EDTA, and 10 μM GDP. To remove the GST tag, PreScission protease was added to the beads at 1:10 (w:w) protease: GST-$G\alpha_s$ ratio and the mixture was rocked overnight at 4 °C with 2 mM DTT. Untagged $G\alpha_s$ was concentrated and further purified by size-exclusion chromatography using a Superdex 200 Increase 10/300 column pre-equilibrated with 20 mM HEPES, pH 7, 150 mM NaCl, 10% glycerol, 5 mM β-mercaptoethanol, 1 mM $MgCl_2$, 1 mM EDTA, 20 μM GDP. Purified $G\alpha_s$ was concentrated to 6 mg/ml, flash frozen in liquid nitrogen and stored at −80 °C.

Bovine $G\beta_1$ and bovine His_6-tagged soluble $G\gamma_2$(C68S) were co-expressed and purified from Sf9 insect cells. 25 ml of each baculovirus were co-infected into Sf9 cells when the insect cell culture reached a cell density at 3 million cells per ml. 48 hrs post infection, cells were harvested by centrifugation, flash frozen in liquid nitrogen and stored at −80 °C. Cell pellets were thawed in 25 mM HEPES pH 7, 150 mM NaCl, 10% glycerol, 2 mM β-mercaptoethanol, 5 mM $MgCl_2$ and protease inhibitor cocktail. Cells were lysed by sonication and cell debris were removed by centrifugation at 142,000 g for 30 min. Supernatant was collected and incubated with Ni-NTA resin with stirring for 1.5 hrs at 4 °C. Resin was then washed three times with 25 mM HEPES pH 7, 150 mM NaCl, 10% glycerol, 2 mM β-mercaptoethanol, and 25 mM imidazole, and $G\beta_1\gamma_2$ was eluted as a complex with 25 mM HEPES pH 7, 150 mM NaCl, 10% glycerol, 2 mM β-mercaptoethanol, and 250 mM imidazole. Eluted protein was concentrated and further purified using a Superdex 200 Increase 10/300 column pre-equilibrated with 25 mM HEPES pH 7, 150 mM NaCl, and 2 mM β-mercaptoethanol. Purified $G\beta_1\gamma_2$ protein was concentrated to 8 mg/ml, flash frozen in liquid nitrogen and stored at −80 °C.

Nb35-His_6 was expressed in the periplasm of *E. coli* strain BL21(DE3). Cells were grown in LB medium (MP Biomedicals) at 37 °C until OD_{600} reached 0.6. Protein expression was then induced by 75 μM IPTG and Nb35 was further expressed for 18 hrs at 16 °C. Cells were then harvested, flash frozen in liquid nitrogen and stored at −80 °C. For protein purification, cells were lysed by sonication in a lysis buffer containing 20 mM HEPES pH 7, 100 mM NaCl, 5 mM $MgCl_2$, 0.1 mM lysozyme, and protease inhibitor cocktail. After removal of the cell debris by centrifugation at 20,000 g for 30 min, supernatant was collected and incubated with Ni-NTA resin with stirring for 1.5 hrs at 4 °C. Resin was then washed three times with 20 mM HEPES pH 7, 100 mM NaCl, and 25 mM imidazole. Nb35

was eluted with 20 mM HEPES pH 7, 100 mM NaCl, and 250 mM imidazole. Eluted Nb35 protein was dialyzed against 1 L of 20 mM HEPES pH 7, 100 mM NaCl overnight at 4 °C. Dialyzed protein was concentrated to 3 mg/ml, flash frozen in liquid nitrogen and stored in −80 °C.

Protein complex assembly and purification: To assemble the β_1-AR-Gs-Nb35 complex, $G\alpha_s$, $G\beta_1\gamma_2$ and Nb35 were mixed at 1:1:1.5 molar ratios in the presence of 2 mM $MgCl_2$. The mixture was incubated for 30 min at room temperature and then mixed with β_1-AR at 1.2:1 ratio. The mixture was diluted with 160 μl buffer containing 10 mM HEPES pH 7, 100 mM NaCl, 0.1 mM TCEP, 0.02% LMNG, 1 mM isoproterenol, and 2 mM $MgCl_2$ to bring the volume to 600 μl. This mixture was incubated for another 30 min at room temperature before 0.4 U Apyrase (Sigma) was added. After additional 30 min room temperature incubation with Apyrase, the mixture was centrifuged at 16,000 g for 10 min to remove any precipitants. The supernatant was then loaded onto a Superdex 200 Increase 10/300 column pre-equilibrated with 10 mM HEPES pH 7, 100 mM NaCl, 0.1 mM TCEP, 0.02% LMNG and 40 uM isoproterenol. The elution fractions from a single peak containing pure β_1-AR-Gs-Nb35 complex was concentrated to ~1.5 mg/ml and used directly for making cryo-EM grids.

Cryo-EM data collection: 4 μl of protein complex was applied to a glow-discharged 400 mesh gold Quantifoil R1.2/1.3 holey carbon grids (Quantifoil Micro Tools), and subsequently vitrified using Vitrobot Mark IV (Thermo Fisher Scientific/FEI). Images were collected at liquid nitrogen temperature on a Titan Krios electron microscope (Thermo Fisher Scientific/FEI) operated at 300 kV accelerating voltage, at a nominal magnification of 22,500× using a Gatan K3 direct electron detector (Gatan, Inc.), corresponding to a super-resolution pixel size of 0.532 Å/pixel at the detector. In total, 5633 micrographs with defocus values in the range of −1.0 μm to −2.3 μm were recorded. Images were recorded as 40 dose-fractionated frames with a total accumulated dose of 46 $e^-/Å^2$.

Image processing, 3D reconstructions, modeling and refinement: Super-resolution movies were aligned and two-times Fourier cropped using MotionCorr2 1.2.1 (Zheng et al., 2017) resulting in a final pixel size of 1.064 Å/pixel. Relion 3.0b2 (Zivanov et al., 2018) Laplacian-of-Gaussian picking with minimum and maximum dimensions of 76 Å and 119 Å was used to heavily over-pick at a rate of approximately 2300 particles per micrograph. False positives were excluded from the particle stack of 13 million particles through multiple rounds of heterogeneous classification using Fourier cropped particles in CryoSparc v2.12.4 (Punjani et al., 2017) (Figure S2). 2D classification was applied to confirm that the excluded particles corresponded to false positives, free receptors or free G-protein heterotrimers. Iterative classification resulted in a stack of intact complexes was 1.5 million particles. Starting from this point, multiple classification strategies in both Relion 3.0b2 and CryoSparc v2.12.4 were used to confirm that there was only one major conformation present in each data set. Further classification converged to a final high resolution stack of 452,312 particles that was then subjected to Local CTF Refinement procedures in CryoSparc v2.12.4 followed by Bayesian Polishing in Relion 3.0b2, and finally Global CTF Refinement in CryoSparc v2.12.4 to improve higher order aberrations (Figure S2). Final high-resolution

reconstructions were subjected to Local Refinement with Non-Uniform Refinement in CryoSparc v2.12.4 for β_1-AR and G-proteins independently. The Local Refinement maps showed significantly improved features over the consensus maps, both with resolutions at or below 2.6 Å (Figure S2). The resulting maps were super-sampled in Coot v0.8.9.2 (Emsley and Cowtan, 2004) to 0.532 Å per pixel with a 512 voxel box. The initial models of β_1-AR and $G\beta_1\gamma_2$ were derived from the crystal structures of inactive β_1-AR (PDB ID: 4GPO) and $G\alpha_q$-GRK2-$G\beta_1\gamma_2$ complex (PDB ID: 2BCJ), respectively.

$G\alpha_s$ and Nb35 were derived from the crystal structures of β_2-AR–Gs complex (PDB ID: 3SN6). The models were manually rebuilt into the focus-refined density maps and refined in real space using Phenix v1.17.1-3660 (Adams et al., 2010). The density of the α-helical domain of $G\alpha_s$ was poor; the α-helical domain from PDB 3SN6 was manually docked into the density and rigid-body fit in COOT. Once refinement converged, enabling a final combined map was derived from the model and the two super-sampled local refinement maps using the Combine Focused Maps feature in Phenix v1.17.1-3660. Since all local and consensus refinements gave gold-standard FSC values of 2.6 Å, we approximate the resolution of this combined consensus map to be 2.6 Å as well (Figure S2). A final round of real space refinement in Phenix v1.17.1-3660 against the combined map yielded the final model.

cAMP assay: CHO-K1 (ATCC) cells were plated onto six-well plates and treated with 1 mM IBMX (Cayman) for 30 min. After washing twice with HEM buffer (20 mM HEPES, pH 7.4, 135 mM NaCl, 4.7 mM KCl, 1.2 mM $MgSO_4$, 2.5 mM $NaHCO_3$, 0.1 mM Ro-20-1724 (Sigma), 0.5 U/ml adenosine deaminase (Roche), and 1 mM IBMX), cells were treated with different concentrations of isoproterenol in HEM buffer for 5 min. After two more washes with HEM buffer, cells were harvested in 0.5% Triton X-100 (Sigma) containing 1 mM IBMX. The amount of cAMP was measured with the Direct Cyclic AMP Enzyme Immunoassay kit (Enzo Life Sciences).

Quantification and Statistical Analysis: In Figure 7C, the cAMP assays were repeated three times, and the data are represented as mean ± SD of the three independent experiments. In Figure 7D, the analysis was done using the log(agonist) vs. response function of Prism 8 (GraphPad) as indicated in the figure legend. Cryo-EM data collection and refinement statistics are listed in Table 1.

Supplementary Material

Refer to Web version on PubMed Central for supplementary material.

ACKNOWLEDGMENTS:

We thank members of our research groups for helpful discussion and comments on the manuscript. This work was supported by an NIH grant HL130478 (X.Y.H.), the Josie Robertson Investigators Program (R.K.H.), the Searle Scholars Program (R.K.H), the Canada Excellence Research Chairs program (O.P.E.), and CIHR grant 159464 (O.P.E.). The Simons Electron Microscopy Center and the National Resource for Automated Molecular Microscopy located at the New York Structural Biology Center is supported by grants from the NIH National Institute of General Medical Sciences (GM103310), NYSTAR, and the Simons Foundation (SF349247).

REFERENCES

Adams PD, Afonine PV, Bunkoczi G, Chen VB, Davis IW, Echols N, Headd JJ, Hung LW, Kapral GJ, Grosse-Kunstleve RW, et al. (2010). PHENIX: a comprehensive Python-based system for macromolecular structure solution. Acta Crystallogr D Biol Crystallogr 66, 213–221. [PubMed: 20124702]

Aurora R, and Rose GD (1998). Helix capping. Protein science : a publication of the Protein Society 7, 21–38. [PubMed: 9514257]

Aurora R, Srinivasan R, and Rose GD (1994). Rules for alpha-helix termination by glycine. Science 264, 1126–1130. [PubMed: 8178170]

Benovic JL (2002). Novel beta2-adrenergic receptor signaling pathways. J Allergy Clin Immunol 110, S229–235. [PubMed: 12464929]

Bos JL, Rehmann H, and Wittinghofer A (2007). GEFs and GAPs: critical elements in the control of small G proteins. Cell 129, 865–877. [PubMed: 17540168]

Bourne HR (1997). How receptors talk to trimeric G proteins. Curr Opin Cell Biol 9, 134–142. [PubMed: 9069253]

Bourne HR, Sanders DA, and McCormick F (1990). The GTPase superfamily: a conserved switch for diverse cell functions. Nature 348, 125–132. [PubMed: 2122258]

Cherezov V, Rosenbaum DM, Hanson MA, Rasmussen SG, Thian FS, Kobilka TS, Choi HJ, Kuhn P, Weis WI, Kobilka BK, et al. (2007). High-resolution crystal structure of an engineered human beta2-adrenergic G protein-coupled receptor. Science 318, 1258–1265. [PubMed: 17962520]

Coleman DE, Berghuis AM, Lee E, Linder ME, Gilman AG, and Sprang SR (1994). Structures of active conformations of Gi alpha 1 and the mechanism of GTP hydrolysis. Science 265, 1405–1412. [PubMed: 8073283]

Conklin BR, and Bourne HR (1993). Structural elements of G alpha subunits that interact with G beta gamma, receptors, and effectors. Cell 73, 631–641. [PubMed: 8388779]

Conklin BR, Farfel Z, Lustig KD, Julius D, and Bourne HR (1993). Substitution of three amino acids switches receptor specificity of Gq alpha to that of Gi alpha. Nature 363, 274–276. [PubMed: 8387644]

Dohlman HG, and Jones JC (2012). Signal activation and inactivation by the Galpha helical domain: a long-neglected partner in G protein signaling. Sci Signal 5, re2. [PubMed: 22649098]

Draper-Joyce CJ, Khoshouei M, Thal DM, Liang YL, Nguyen ATN, Furness SGB, Venugopal H, Baltos JA, Plitzko JM, Danev R, et al. (2018). Structure of the adenosinebound human adenosine A1 receptor-Gi complex. Nature 558, 559–563. [PubMed: 29925945]

Dror RO, Mildorf TJ, Hilger D, Manglik A, Borhani DW, Arlow DH, Philippsen A, Villanueva N, Yang Z, Lerch MT, et al. (2015). SIGNAL TRANSDUCTION. Structural basis for nucleotide exchange in heterotrimeric G proteins. Science 348, 1361–1365. [PubMed: 26089515]

Emsley P, and Cowtan K (2004). Coot: model-building tools for molecular graphics. Acta Crystallogr D Biol Crystallogr 60, 2126–2132. [PubMed: 15572765]

Fredriksson R, Lagerstrom MC, Lundin LG, and Schioth HB (2003). The G-protein-coupled receptors in the human genome form five main families. Phylogenetic analysis, paralogon groups, and fingerprints. Mol Pharmacol 63, 1256–1272. [PubMed: 12761335]

Frishman WH (2008). beta-Adrenergic blockers: a 50-year historical perspective. Am J Ther 15, 565–576. [PubMed: 19127141]

Gilman AG (1987). G proteins: transducers of receptor-generated signals. Annu Rev Biochem 56, 615–649. [PubMed: 3113327]

Herrmann R, Heck M, Henklein P, Hofmann KP, and Ernst OP (2006). Signal transfer from GPCRs to G proteins: role of the G alpha N-terminal region in rhodopsin-transducin coupling. J Biol Chem 281, 30234–30241. [PubMed: 16847064]

Hilger D, Masureel M, and Kobilka BK (2018). Structure and dynamics of GPCR signaling complexes. Nat Struct Mol Biol 25, 4–12. [PubMed: 29323277]

Huang J, Chen S, Zhang JJ, and Huang XY (2013). Crystal structure of oligomeric beta1-adrenergic G protein-coupled receptors in ligand-free basal state. Nat Struct Mol Biol 20, 419–425. [PubMed: 23435379]

Huang J, Sun Y, Zhang JJ, and Huang XY (2015). Pivotal role of extended linker 2 in the activation of Galpha by G protein-coupled receptor. J Biol Chem 290, 272–283. [PubMed: 25414258]

John J, Sohmen R, Feuerstein J, Linke R, Wittinghofer A, and Goody RS (1990). Kinetics of interaction of nucleotides with nucleotide-free H-ras p21. Biochemistry 29, 6058–6065. [PubMed: 2200519]

Kang Y, Kuybeda O, de Waal PW, Mukherjee S, Van Eps N, Dutka P, Zhou XE, Bartesaghi A, Erramilli S, Morizumi T, et al. (2018). Cryo-EM structure of human rhodopsin bound to an inhibitory G protein. Nature 558, 553–558. [PubMed: 29899450]

Koehl A, Hu H, Maeda S, Zhang Y, Qu Q, Paggi JM, Latorraca NR, Hilger D, Dawson R, Matile H, et al. (2018). Structure of the micro-opioid receptor-Gi protein complex. Nature 558, 547–552. [PubMed: 29899455]

Lambright DG, Sondek J, Bohm A, Skiba NP, Hamm HE, and Sigler PB (1996). The 2.0 A crystal structure of a heterotrimeric G protein. Nature 379, 311–319. [PubMed: 8552184]

Lappano R, and Maggiolini M (2012). GPCRs and cancer. Acta Pharmacol Sin 33, 351–362. [PubMed: 22266725]

Liang YL, Khoshouei M, Glukhova A, Furness SGB, Zhao P, Clydesdale L, Koole C, Truong TT, Thal DM, Lei S, et al. (2018). Phase-plate cryo-EM structure of a biased agonist-bound human GLP-1 receptor-Gs complex. Nature 555, 121–125. [PubMed: 29466332]

Liang YL, Khoshouei M, Radjainia M, Zhang Y, Glukhova A, Tarrasch J, Thal DM, Furness SGB, Christopoulos G, Coudrat T, et al. (2017). Phase-plate cryo-EM structure of a class B GPCR-G-protein complex. Nature 546, 118–123. [PubMed: 28437792]

Lohse MJ, Engelhardt S, and Eschenhagen T (2003). What is the role of beta-adrenergic signaling in heart failure? Circ Res 93, 896–906. [PubMed: 14615493]

Markby DW, Onrust R, and Bourne HR (1993). Separate GTP binding and GTPase activating domains of a G alpha subunit. Science 262, 1895–1901. [PubMed: 8266082]

Noel JP, Hamm HE, and Sigler PB (1993). The 2.2 A crystal structure of transducin-alpha complexed with GTP gamma S. Nature 366, 654–663. [PubMed: 8259210]

Oldham WM, and Hamm HE (2008). Heterotrimeric G protein activation by G-protein-coupled receptors. Nat Rev Mol Cell Biol 9, 60–71. [PubMed: 18043707]

Post SR, Hammond HK, and Insel PA (1999). Beta-adrenergic receptors and receptor signaling in heart failure. Annu Rev Pharmacol Toxicol 39, 343–360. [PubMed: 10331088]

Punjani A, Rubinstein JL, Fleet DJ, and Brubaker MA (2017). cryoSPARC: algorithms for rapid unsupervised cryo-EM structure determination. Nat Methods 14, 290–296. [PubMed: 28165473]

Rasmussen SG, DeVree BT, Zou Y, Kruse AC, Chung KY, Kobilka TS, Thian FS, Chae PS, Pardon E, Calinski D, et al. (2011). Crystal structure of the beta2 adrenergic receptor-Gs protein complex. Nature 477, 549–555. [PubMed: 21772288]

Rosenbaum DM, Rasmussen SG, and Kobilka BK (2009). The structure and function of G-protein-coupled receptors. Nature 459, 356–363. [PubMed: 19458711]

Sakmar TP (2002). Structure of rhodopsin and the superfamily of seven-helical receptors: the same and not the same. Curr Opin Cell Biol 14, 189–195. [PubMed: 11891118]

Simon MI, Strathmann MP, and Gautam N (1991). Diversity of G proteins in signal transduction. Science 252, 802–808. [PubMed: 1902986]

Sprang SR (1997). G protein mechanisms: insights from structural analysis. Annu Rev Biochem 66, 639–678. [PubMed: 9242920]

Sprang SR, Chen Z, and Du X (2007). Structural basis of effector regulation and signal termination in heterotrimeric Galpha proteins. Adv Protein Chem 74, 1–65. [PubMed: 17854654]

Strange PG (2008). Signaling mechanisms of GPCR ligands. Curr Opin Drug Discov Devel 11, 196–202.

Sunahara RK, Tesmer JJ, Gilman AG, and Sprang SR (1997). Crystal structure of the adenylyl cyclase activator Gsalpha [see comments]. Science 278, 1943–1947. [PubMed: 9395396]

Wall MA, Coleman DE, Lee E, Iniguez-Lluhi JA, Posner BA, Gilman AG, and Sprang SR (1995). The structure of the G protein heterotrimer Gi alpha 1 beta 1 gamma 2. Cell 83, 1047–1058. [PubMed: 8521505]

Warne T, Serrano-Vega MJ, Baker JG, Moukhametzianov R, Edwards PC, Henderson R, Leslie AG, Tate CG, and Schertler GF (2008). Structure of a beta1-adrenergic G-protein-coupled receptor. Nature 454, 486–491. [PubMed: 18594507]

Weis WI, and Kobilka BK (2018). The Molecular Basis of G Protein-Coupled Receptor Activation. Annu Rev Biochem 87, 897–919. [PubMed: 29925258]

Zhang Y, Sun B, Feng D, Hu H, Chu M, Qu Q, Tarrasch JT, Li S, Sun Kobilka T, Kobilka BK, et al. (2017). Cryo-EM structure of the activated GLP-1 receptor in complex with a G protein. Nature 546, 248–253. [PubMed: 28538729]

Zheng SQ, Palovcak E, Armache JP, Verba KA, Cheng Y, and Agard DA (2017). MotionCor2: anisotropic correction of beam-induced motion for improved cryo-electron microscopy. Nat Methods 14, 331–332. [PubMed: 28250466]

Zivanov J, Nakane T, Forsberg BO, Kimanius D, Hagen WJ, Lindahl E, and Scheres SH (2018). New tools for automated high-resolution cryo-EM structure determination in RELION-3. Elife 7.

Highlights:

- Cryo-EM structure of β_1-adrenergic receptor and Gs at 2.6 Å resolution
- Network of interactions within $G\alpha_s$ are disrupted by β_1-AR
- Rotational opening of the α-helical domain of $G\alpha_s$ during its activation
- Functional studies of critical residues on β_1-AR involved in the activation of Gs

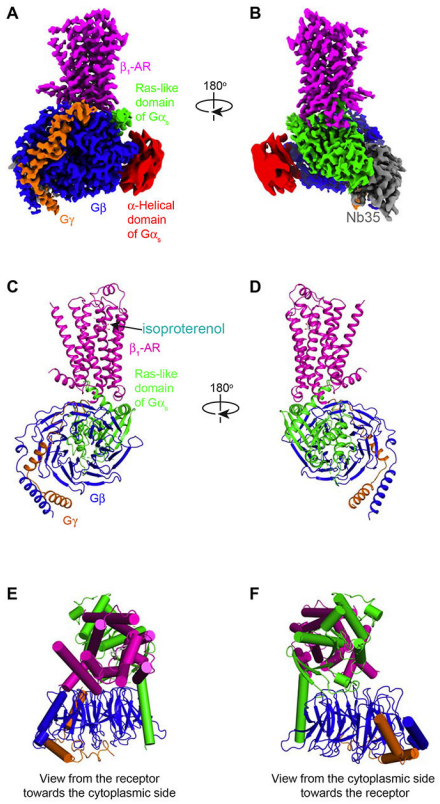

Figure 1. Overall architecture of the structure of the isoproterenol–β_1-AR–Gs complex.

(**A,B**) Orthogonal views of the cryo-EM density map of the isoproterenol–β_1-AR–Gs complex colored by subunits (β_1-AR in magenta, Ras-like GTPase domain of Gα_s in green, α-helical domain of Gα_s in red (low-pass filtered to 6 Å for better presentation), Gβ in blue, Gγ in orange, and Nb35 in gray). (**C,D**) Cartoon diagrams of the isoproterenol–β_1-AR–Gs complex are shown without Nb35 and the α-helical domain of Gα_s. Color schemes are the same as in **A** and **B**. (**E,F**) Extracellular and cytoplasmic views of the isoproterenol–β_1-AR–Gs complex.

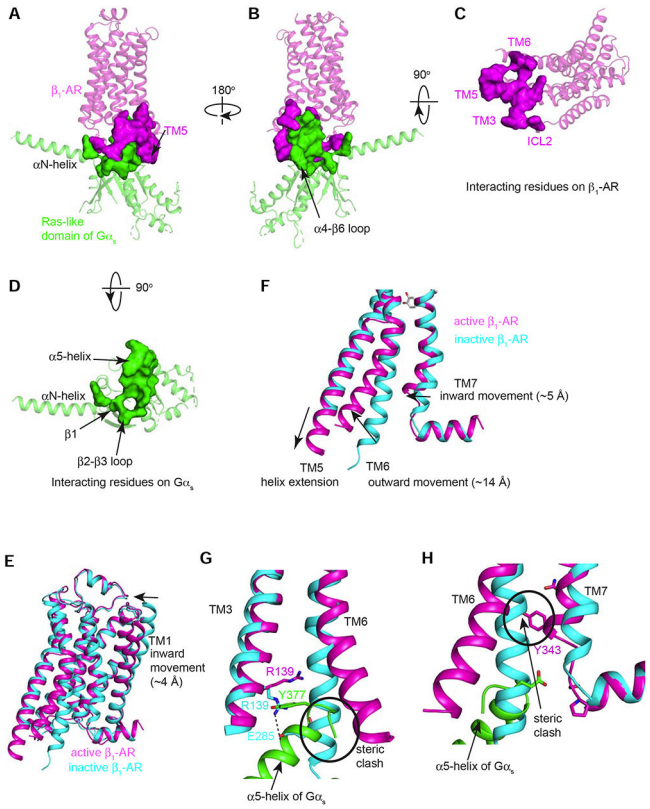

Figure 2. Molecular recognition of Gs by β_1-AR.

(**A-D**) Different views of the interaction surface areas between β_1-AR (in magenta) and the Ras-like GTPase domain of $G\alpha_s$ (in green) are shown. (**E-H**) Comparison of the conformations of β_1-AR in the active state (magenta) as seen in the β_1-AR–Gs complex and with that of β_1-AR in the inactive state (PDB: 4GPO) (cyan). (**E**) The overall alignment of the inactive β_1-AR and the active β_1-AR. (**F**) Major conformational changes in TM5, TM6 and TM7. (**G** and **H**) Conformational changes in the conserved D(E)RY motif on TM3 (**G**) and the conserved NPxxY motif on TM7 (**H**).

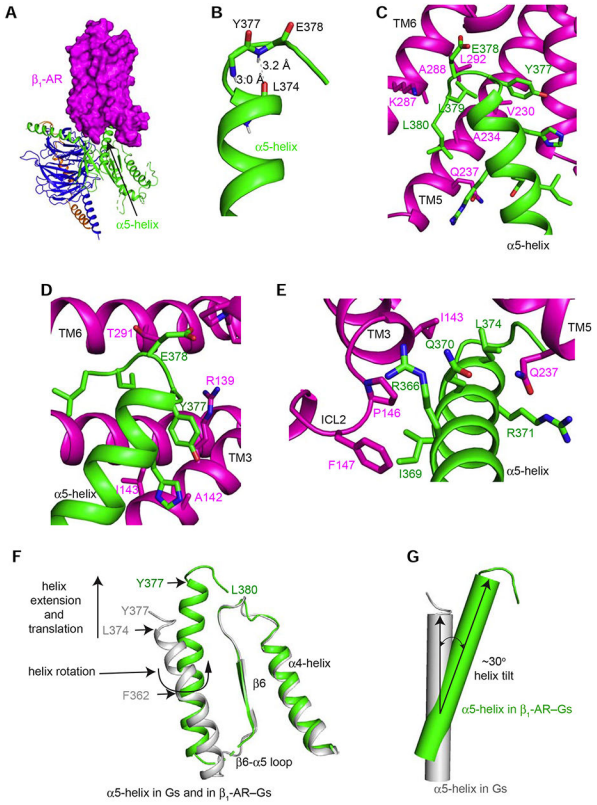

Figure 3. Structural rearrangements of the α5-helix of $G\alpha_s$ upon binding of β_1-AR.

(**A**) β_1-AR uses its cytoplasmic surface like a saddle to cradle the C-terminal α5-helix of the Ras-like domain of $G\alpha_s$. (**B**) The last 4 amino acids (Tyr377 to Leu380) of α5-helix form a C-terminal α_L capping motif with intra-chain interactions. (**C** and **D**) Interactions between β_1-AR and the C-terminal tail loop of the α5-helix of $G\alpha_s$. (**E**) Interactions between the middle of the α5-helix of $G\alpha_s$ and β_1-AR. (**F**) Structural comparison of the α5-helix of $G\alpha_s$ from the β_1-AR–Gs complex (colored in green) and from $G\alpha_s$-GTPγS (colored in gray). (**G**) Tilting of the α5-helix of $G\alpha_s$ from $G\alpha_s$-GTPγS (colored in gray) to the β_1-AR–Gs complex (colored in green).

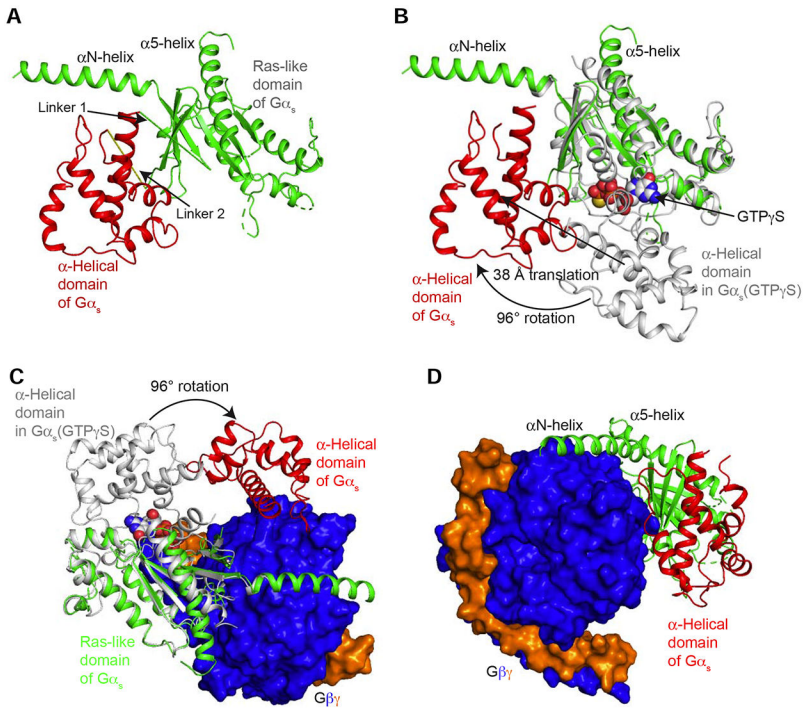

Figure 4. Rotational opening of the α-helical domain of $G\alpha_s$ during its activation by β_1-AR.

(**A)** Structure of $G\alpha_s$ in the complex of β_1-AR–Gs shows the open rotation of the α-helical domain from the Ras-like domain. (**B)** Comparison of the structures of $G\alpha_s$ in the complex of β_1-AR–Gs (in green and red) and in the $G\alpha_s$:GTPγS crystal structure (in gray). (**C**) View from the receptor towards the cytoplasmic end shows the rotation of the α-helical domain from the position in the $G\alpha_s$:GTPγS crystal structure (in gray) to the location in the β_1-AR–Gs complex (in red). (**D**) View from Gβγ towards the Ras-like domain shows the position of the α-helical domain relative to Gβ.

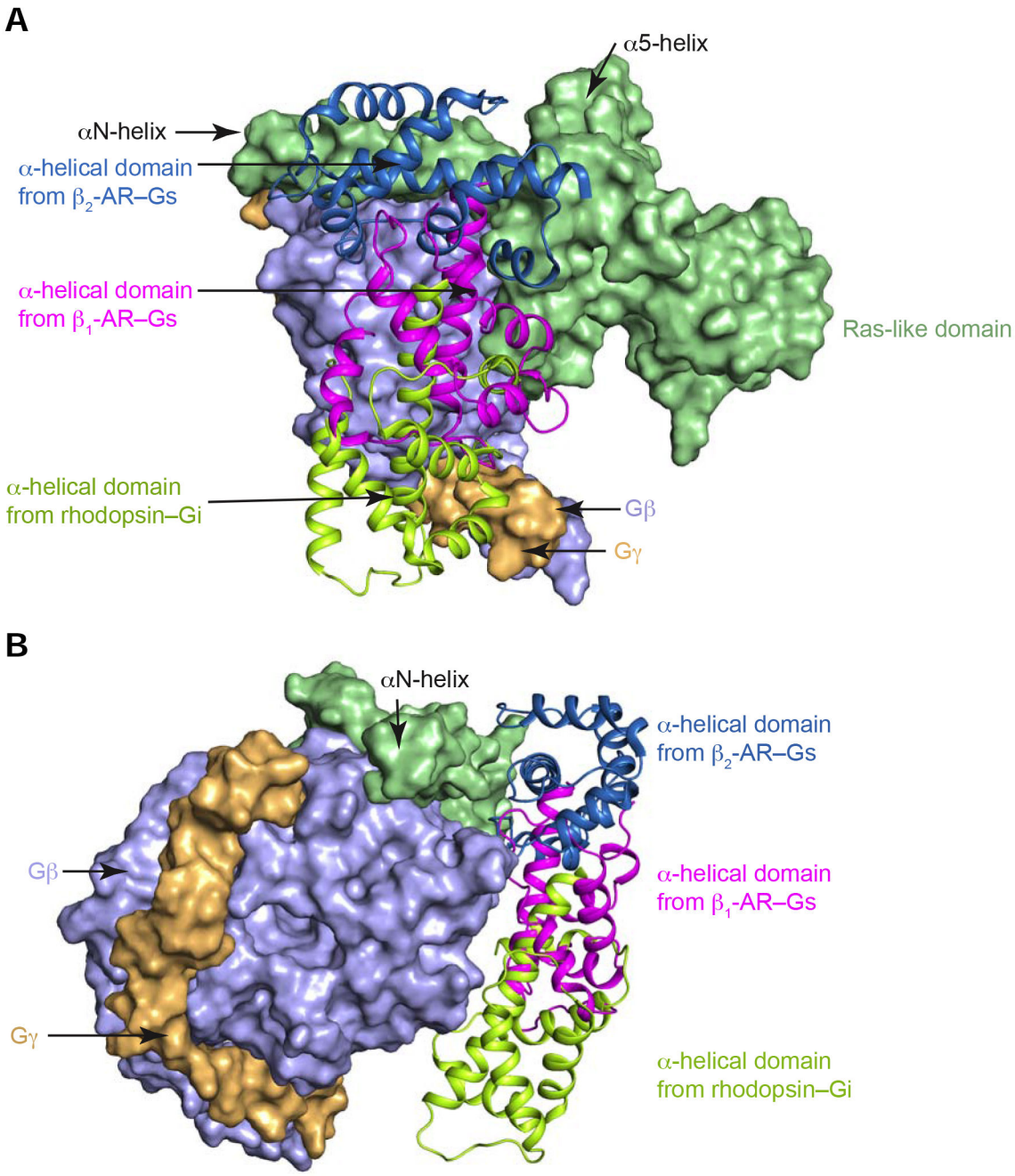

Figure 5. Comparison of the locations of the α-helical domains from the structures of the complexes of BI-167107-activated β_2-AR–Gs (in skyblue), isoproterenol-activated β_1-AR–Gs (in magenta), and constitutively active rhodopsin–Gi (in limon).

The Ras-like domains (in light green), Gβ (in light blue) and Gγ (in light orange) from the three complexes were superimposed and presented in surface diagram. **A** and **B** show different views.

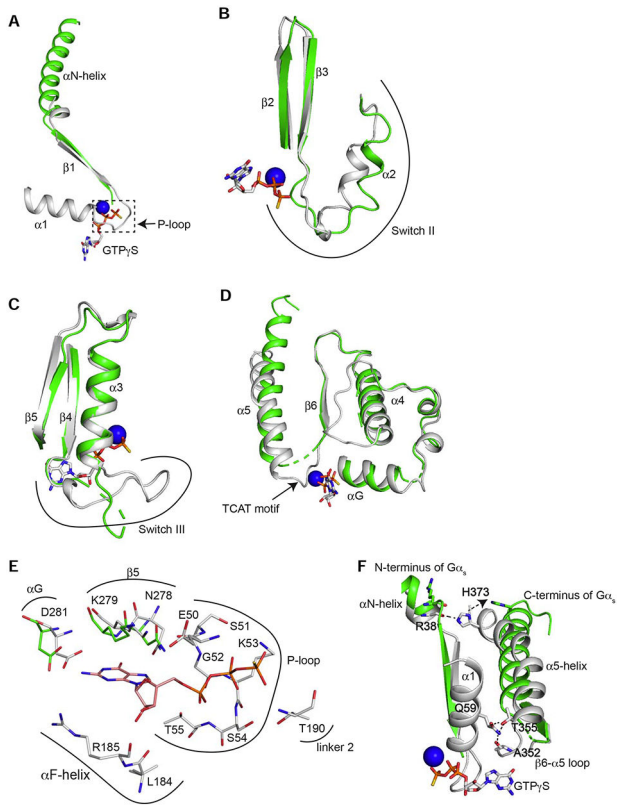

Figure 6. Conformational changes of the GDP/GTP-binding pocket after β_1-AR interaction.

(A) Comparison of the β_1 strand, α_1-helix and the β_1-α_1 loop of the Ras-like domains from β_1-AR–Gs (in green) and from Gα_s:GTPγS (in gray) when the Ras-like domains are superimposed. (**B**) Comparison of Switch II region from β_1-AR–Gs and from Gα_s:GTPγS. (**C**) Comparison of Switch III region from β_1-AR–Gs and from Gα_s:GTPγS. (**D**) Comparison of the regions from αG to α5-helix from β_1-AR–Gs and from Gα_s:GTPγS. (**E**) Comparison of all GTP-interacting residues of the Ras-like domains from β_1-AR–Gs and from Gα_s:GTPγS. (**F**) Disruptions of intramolecular interactions of Gα_s during Gs activation by β_1-AR. An ionic lock between the sidechain of His373 in the α5-helix and the backbone carbonyl of Arg38 in the αN-helix is broken. An interacting network involving the sidechain of Gln59 in the α1-helix, the backbone carbonyl of Ala352 in the β6-α5 loop, and the sidechain of Thr355 in the α5-helix is disrupted.

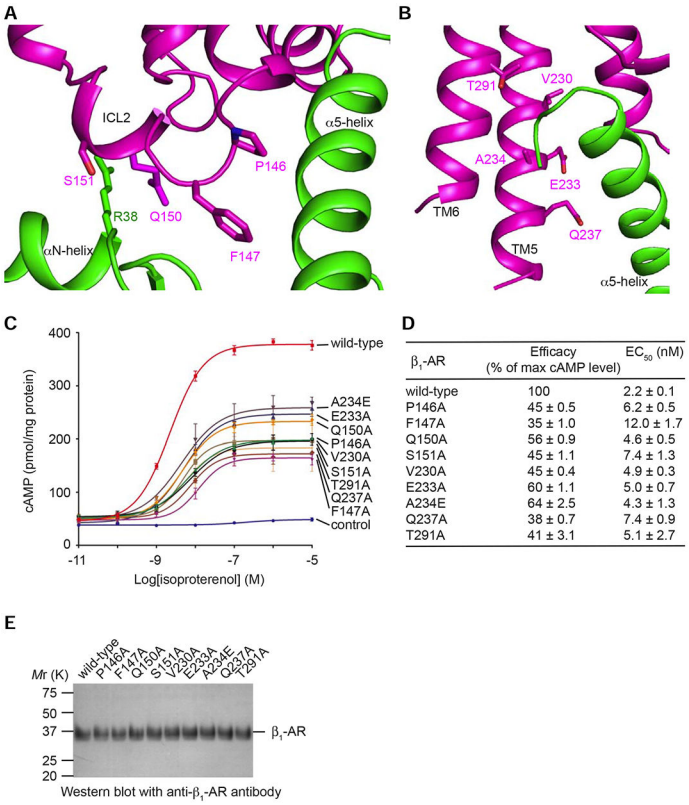

β_1-AR	Efficacy (% of max cAMP level)	EC_{50} (nM)
wild-type	100	2.2 ± 0.1
P146A	45 ± 0.5	6.2 ± 0.5
F147A	35 ± 1.0	12.0 ± 1.7
Q150A	56 ± 0.9	4.6 ± 0.5
S151A	45 ± 1.1	7.4 ± 1.3
V230A	45 ± 0.4	4.9 ± 0.3
E233A	60 ± 1.1	5.0 ± 0.7
A234E	64 ± 2.5	4.3 ± 1.3
Q237A	38 ± 0.7	7.4 ± 0.9
T291A	41 ± 3.1	5.1 ± 2.7

Figure 7. Functional studies of specific interacting residues in Gs activation by β_1-AR.

(**A** and **B**) Locations of the mutated residues in ICL2 and in the TM5-ICL3-TM6 region of β_1-AR. (**C**) Dose-response data from cells expressing different β_1-ARs after stimulation with isoproterenol. Data are represented as mean ± SD of three experiments. (**D**) Summary of the efficacy (the maximum cAMP level of a mutant receptor / the maximum cAMP level of the wild-type receptor) and EC_{50} values based on the cAMP assay data shown in **C**. Data are represented as mean ± SD of three experiments. The analysis was done using the log(agonist) vs. response function of Prism 8 (GraphPad). (**E**) Western blots of same amounts of total proteins from membrane preparations of cells transfected with wild-type and mutant β_1-ARs with anti-β_1-AR antibody show similar expression levels of the receptor proteins.

Table 1.

Cryo-EM data collection, refinement and validation statistics

Data collection and processing	
Magnification	22,500
Voltage (kV)	300
Electron exposure (e–/Å^2)	46
Defocus range (μm)	−1.0 to −2.3
Pixel size (Å)	1.064
Symmetry imposed	C1
Initial particle images (no.)	1,498,944
Final particle images (no.)	452,312
Map resolution (Å) (Full /G-protein	
focus /β_1-AR focus)	2.58/2.58/2.56
FSC threshold	0.143
Refinement	
Model resolution (Å)	2.32/2.68
FSC threshold	0.143/0.50
Map sharpening B factor (Å^2)	−80
Model composition	
Non-hydrogen atoms	7902
Protein residues	1004
Ligands	1
B factors (Å^2)	54.0
R.m.s. deviations	
Bond lengths (Å)	0.002
Bond angles (°)	0.455
Validation	
MolProbity score	1.27
Clashscore	2.81
Poor rotamers (%)	1.78
Ramachandran plot	
Favored (%)	97.96
Allowed (%)	2.04
Disallowed (%)	0.00

KEY RESOURCES TABLE

REAGENT or RESOURCE	SOURCE	IDENTIFIER
Bacterial and Virus Strains		
E. coli strain BL21(DE3)	New England Biolabs	Cat# C2527H
Recombinant baculovirus for $G\beta_1$	Huang et al., 2015	N/A
Recombinant baculovirus for $G\gamma_2$(C68S)	Huang et al., 2015	N/A
Chemicals, Peptides, and Recombinant Proteins		
ESF 921 protein-free medium	Expression Systems	Cat# 96-001-01
Protease inhibitor cocktail	Roche	Cat# 5892791001
Isoproterenol	Sigma	Cat# I6504
DDM	Anatrace	Cat# D310S
LMNG	Anatrace	Cat# NG310
2×YT medium	MP Biomedicals	Cat# 113012042
IPTG	GoldBio	Car# I2481C
GDP	Sigma	Cat# G7127
PreScission protease	Prepared In-House	N/A
LB medium	MP Biomedicals	Cat# 113002042
Apyrase	Sigma	Cat# A6237
IBMX	Cayman	Cat# 13347
Ro-20-1724	Sigma	Cat# B8279
Adenosine deaminase	Roche	Cat# 10102105001
Triton X-100	Sigma	Cat# X100
Critical Commercial Assays		
Direct Cyclic AMP Enzyme Immunoassay kit	Enzo Life Sciences	Cat# ADI-900-066
Deposited Data		
β_1-AR-Gs-Nb35 coordinates	This paper	PDB: 7JJO
β_1-AR-Gs-Nb35 EM map	This paper	EMDB: EMD-22357
Experimental Models: Cell Lines		
Insect cell line Sf9	Expression Systems	Cat# 94-001S
CHO-K1	ATCC	Cat# CCL-61
Recombinant DNA		
pVL1391-β_1-AR (H12)	This paper	N/A
pGEX-6P-$G\alpha_s$	Huang et al., 2015	N/A
pET-26b-Nb35	This paper	N/A
pcDNA3.1-β_1-AR (H0)	Huang et al., 2013	N/A
pcDNA3.1-β_1-AR (H0) (P146A)	This paper	N/A
pcDNA3.1-β_1-AR (H0) (F147A)	This paper	N/A
pcDNA3.1-β_1-AR (H0) (Q150A)	This paper	N/A

REAGENT or RESOURCE	SOURCE	IDENTIFIER
pcDNA3.1-β_1-AR (H0) (S151A)	This paper	N/A
pcDNA3.1-β_1-AR (H0) (V230A)	This paper	N/A
pcDNA3.1-β_1-AR (H0) (E233A)	This paper	N/A
pcDNA3.1-β_1-AR (H0) (A234E)	This paper	N/A
pcDNA3.1-β_1-AR (H0) (Q237A)	This paper	N/A
pcDNA3.1-β_1-AR (H0) (T291A)	This paper	N/A
Software and Algorithms		
MotionCorr2 1.2.1	Zheng et al., 2017	https://msg.ucsf.edu/software
Relion 3.0b2	Zivanov et al., 2018	https://www3.mrc-lmb.cam.ac.uk/relion/index.php/Download_%26_install
CryoSparc v2.12.4	Punjani et al., 2017	https://cryosparc.com/
Coot v0.8.9.2	Emsley and Cowtan, 2004	https://www2.mrc-lmb.cam.ac.uk/personal/pemsley/coot/
Phenix v1.17.1-3660	Adams et al., 2010	https://www.phenix-online.org/
Other		
Ni-NTA resin	Qiagen	Cat# 30210
Superdex 200 Increase 10/300 column	GE Healthcare	Cat# 28990944
Glutathione resin	Pierce	Cat# 16100
400 mesh gold Quantifoil R1.2/1.3 holey carbon grids	Quantifoil Micro Tools	Cat# Q4100AR1.3